Scaffold hopping via ANCHOR.QUERY

Shaabani, S.; Neochoritis, C. G.; Twarda-Clapa, Aleksandra; Musielak, Bogdan; Holak, Tad A.; Domling, A.

Published in:
MedChemCommun

DOI:
10.1039/c7md00058h

MedChemComm

RESEARCH ARTICLE

View Article Online
View Journal | View Issue

Cite this: *Med. Chem. Commun.*, 2017, **8**, 1046

Received 1st February 2017,
Accepted 8th March 2017

DOI: 10.1039/c7md00058h

rsc.li/medchemcomm

Scaffold hopping *via* ANCHOR.QUERY: β-lactams as potent p53-MDM2 antagonists†‡

S. Shaabani,[ab] C. G. Neochoritis,[a] A. Twarda-Clapa,[cd] B. Musielak,[e] T. A. Holak[de] and A. Dömling *[a]

Using the pharmacophore-based virtual screening platform ANCHOR.QUERY, we morphed our recently described Ugi-4CR scaffold towards a β-lactam scaffold with potent p53-MDM2 antagonizing activities. 2D-HSQC and FP measurements confirm potent MDM2 binding. Molecular modeling studies were used to understand the observed SAR in the β-lactam series.

Introduction

Changing the central scaffold of a small molecule while keeping the key receptor interactions in place is called scaffold hopping and is a very important technique in medicinal chemistry.[1,2] Scaffold hopping can yield improved PKPD properties, affinity and selectivity, or intellectual property. We have recently introduced the pharmacophore-based virtual screening platform ANCHOR.QUERY which allows for the fast and efficient screening of very large chemical libraries based on multicomponent reaction chemistries (MCRs).[3,4] It is particularly useful to search for protein–protein interactions (PPI), where a deeply buried amino acid anchor motif comprises an energetic hot spot. Such an anchor motif is the Trp23 in the triad Phe19-Trp23-Leu26 present in p53-MDM2 PPI.[5] Of the three amino acids of the triad, the central Trp23 is buried most deeply into the MDM2 receptor. Feeding Trp23 as the anchor motif in ANCHOR.QUERY yielded several scaffolds with nM affinity to MDM2.[3,4,6–10] A key feature of the anchor approach is the ease of synthesis of predicted binders, typically by one or two chemical steps employing MCR chemistries.[11,12]

Recently, using this approach, we have discovered a potent Ugi-4CR-based molecule (**1**) which opens up an additional pocket in MDM2, beyond the well-known three finger pharmacophore model.[7,13] Amongst all described,[14] this small molecule is unique as it targets and stabilizes the intrinsically disordered *N*-terminus of MDM2. To explore this binding mode even more, we applied ANCHOR.QUERY as a scaffold hopping tool to discover a novel class of p53-MDM2 antagonists based on a β-lactam scaffold.

Results and discussion

Virtual screening (VS)-based β-lactam scaffold discovery

Scaffolds are often defined by topological computational approaches, *e.g.* Bemis and Murcko (BM scaffolds).[15] Here however, we will use a chemistry-based definition which allows an intuitive immediate application, our recently introduced scaffold definition, "*as the smallest atomic denominator and its connectivity resulting from a reaction or reaction sequence using starting materials with common functional groups.*"[16]

The recently found Ugi-4CR scaffold with an experimentally solved cocrystal structure between MDM2 and a potent derivative **1** (PDB ID 4MDN) was the starting point of the discovery and development of the current inhibitors.[7] β-aminoacylamide **1** (Fig. 1B) binds with a K_i of 600 nM to the MDM2 receptor. Fig. 1A shows the main characteristics of this model. 6-chloroindole-2-carboxylic acid was used as an anchor-building block in order to mimic the Trp23 amino acid. Three additional binding sites Phe19, Leu26 and the induced Leu26 subpocket, enlarged by the Tyr100 'open' position, were filled by *tert*-butyl, benzyl and *p*-chlorobenzyl substituents, respectively. Using our open access pharmacophore-based virtual screening web-platform ANCHOR.QUERY (http://anchorquery.csb.pitt.edu), the aforementioned model was analyzed (Fig. 1A).[4] A 4-point pharmacophore point model is proposed by ANCHOR.QUERY (Fig. 1D). The importance of the different parts of the molecule for binding, especially the *p*-chlorobenzyl groups, was confirmed by the small-network analysis program SCORPION (Fig. 1C).[17] Thus, we used the pharmacophore model, including the TRP anchor, two aromatases and a hydrophobe, to

[a] *Department of Drug Design, University of Groningen, The Netherlands. E-mail: a.s.s.domling@rug.nl*
[b] *Faculty of Chemistry, Shahid Beheshti University, Tehran, Iran*
[c] *Faculty of Biochemistry, Biophysics and Biotechnology, Jagiellonian University, Krakow, Poland*
[d] *Malopolska Centre of Biotechnology, Jagiellonian University, Krakow, Poland*
[e] *Department of Chemistry, Jagiellonian University, Krakow, Poland*

† The authors declare no competing interests.

‡ Electronic supplementary information (ESI) available: General procedures, results of fluorescence polarization binding and NMR studies, characterization data, and exemplary copies of NMR spectra. See DOI: 10.1039/c7md00058h

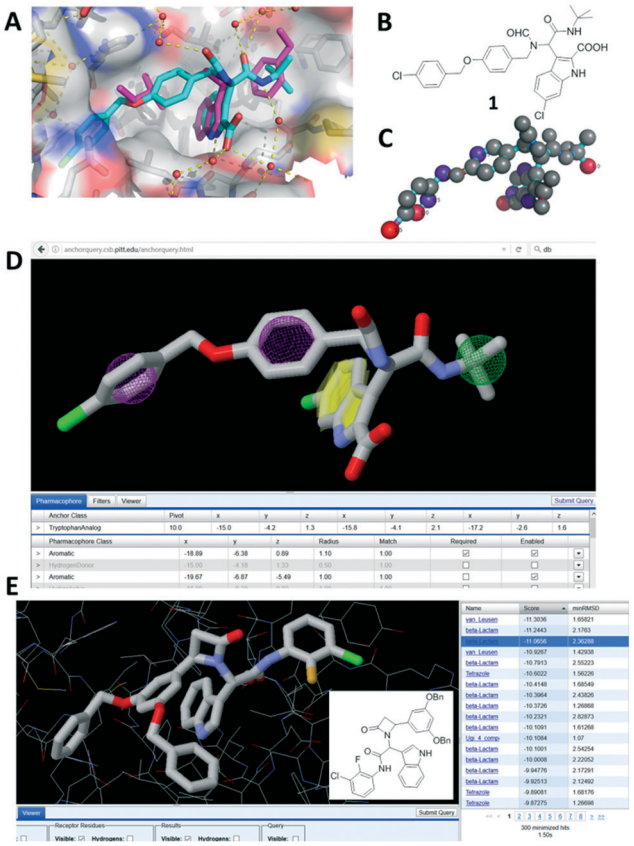

Fig. 1 Process of scaffold hopping using ANCHOR.QUERY. A: Cocrystal structure (PDB ID 4MDN) of **1** (cyan sticks) in MDM2 aligned with the p53-MDM2 structure (PDB ID 1YCR) and showing the only p53 hot spot FYL as pink sticks. B: 2D structure of **1**. C: Scores by the small-network analysis program SCORPION. D: Pharmacophore model of **1** in ANCHOR.QUERY (anchor: yellow, aromatase: pink, hydrophobe: green). E: Top β-lactam result of the pharmacophore search based on **1** with the 2D structure inserted.

query a >30 million virtual compound library based on different MCR scaffolds. An interesting feature of ANCHOR.QUERY is the analysis of the results based on the occurrence of a particular scaffold in the hit list (enrichment factors).

Using this particular pharmacophore model, the observed order of enrichment of scaffolds is shown in Fig. 2. According to occurrence, the top scaffold is the Ugi-β-lactam, followed by the Ugi-tetrazole-3CR scaffold, Ugi-hydantoin, U-4CR,[18] Castagnolli-3CR,[19,20] Doebner-3CR[21] and van Leusen,[22] which are the highest scoring amongst the 27 MCR scaffold space populated with >30 million individual compounds. Several potent MDM2 binders based on these scaffolds and cocrystallized with the MDM2 receptor have been described by us and others in the past.[3,6,7,23] A high-ranking β-lactam compound after energy minimization is shown in Fig. 1E. Based on the promising results of the pharmacophore search, we embarked to synthesize several proposed compounds and derivatives based on the unprecedented Ugi-β-lactam 3CR and investigated their binding behavior to the MDM2/X receptor.

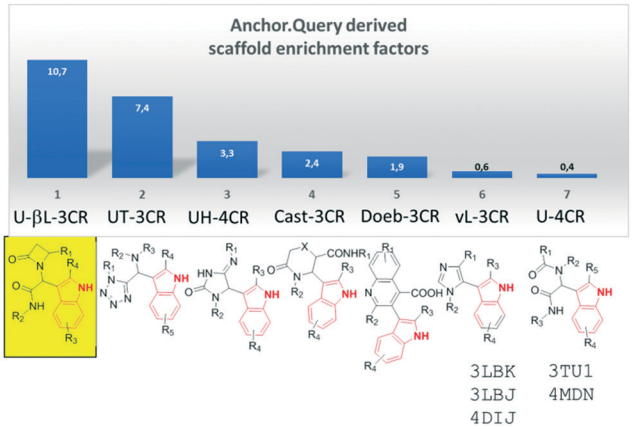

Fig. 2 ANCHOR.QUERY derived scaffold enrichment factors using **1** (Fig. 1D) as a query. The top scoring scaffold is the yellow boxed Ugi-β-lactam 3CR. For the last two scaffolds, several cocrystal structures in MDM2 and MDMX have been published in the past.

Chemistry

The designed scaffold **2** could be easily obtained by a union of two MCRs: α-aminoalkylation to produce the required substituted β-amino acids and Ugi-β-lactam reaction (Scheme 1).[24] The Ugi-β-lactam reaction incorporates the anchoring 3-indolecarboxaldehyde **4**, aliphatic isocyanides **5** and suitably substituted β-aminoacids **6**. Aldehyde **4** was synthesized from the 6-chloro-indole derivative using the Vilsmeier–Haack formylation reaction.[3,6] For the preliminary SAR analysis of the Leu26 pocket and the induced pockets, we synthesized three different substituted β-aminoacids **10a–c** by simply refluxing a mixture of substituted benzaldehydes **7a–c**, malonic acid and ammonium acetate (Scheme 2).[25] The choice of the starting materials was based on our previous results on designing inhibitors of the p53-MDM2/X interaction.[26,27] Concerning the Phe19 pocket, we utilized bulky aliphatic isocyanides, such as the *tert*-butyl (**5a**) and the 1-adamantyl isocyanide (**5b**), which were prepared by the classic dehydration of the corresponding formamide using $POCl_3$.

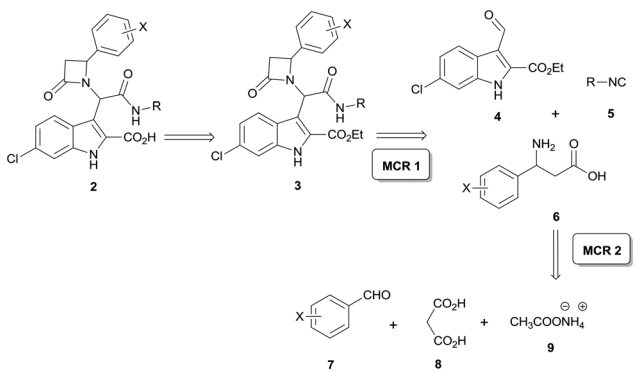

Scheme 1 Retrosynthesis of the targeted β-lactams **2** based on union of two MCRs: 3-component α-aminoalkylation and Ugi-β-lactam reaction.

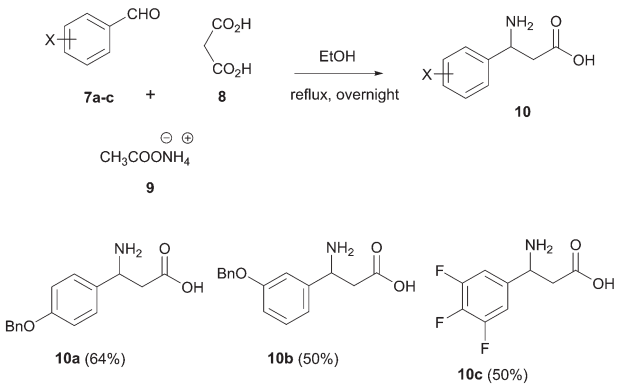

Scheme 2 Synthesis of the substituted β-aminoacids by refluxing the substituted benzaldehydes **7a–c**, malonic acid and ammonium acetate.

Next, we proceeded with the Ugi-β-lactam reaction and the subsequent hydrolysis in total yields of 41–64%. Thus, a mixture of the substituted aminoacids **10a–c**, the 6-chloro-indole carboxaldehyde **4** and the isocyanides **5a** and **b** in trifluoroethanol was irradiated in a microwave oven at 130 °C for 90 min. As expected, we obtained both diastereomers of the desired adducts **3a–e** in a d.r. of ~1 : 1.

In order to better understand the affinity of the final compounds, separation of the diastereomers was necessary. Thus, after careful chromatographic separation, we were able to isolate both diastereomers which were hydrolyzed to the corresponding acids **2a–e**. The hydrolysis of the corresponding esters is necessary based on previous experience with other scaffolds. Esters show an always worse affinity to MDM2 compared to the free carboxylic acid by a factor of 5 or more.[3,7,28–30] To investigate if the chloroindole anchor can be replaced by a *p*-halo phenyl group and following the same synthetic pathway, we also replaced the 6-chloro-indole with a 4-chloro-phenyl group, yielding compounds **2f** and **g** (Scheme 3).

Biophysical screening and structure–activity relationship studies

Two complementary assays based on independent physicochemical principles, fluorescence polarization (FP) and HMQC NMR, were used to exclude false positive hits. Fluorescence polarization (FP) assay was employed to determine the inhibitory affinities (K_i) of tetrazole derivatives against MDM2 and MDMX, as previously described.[31,32] The results are presented

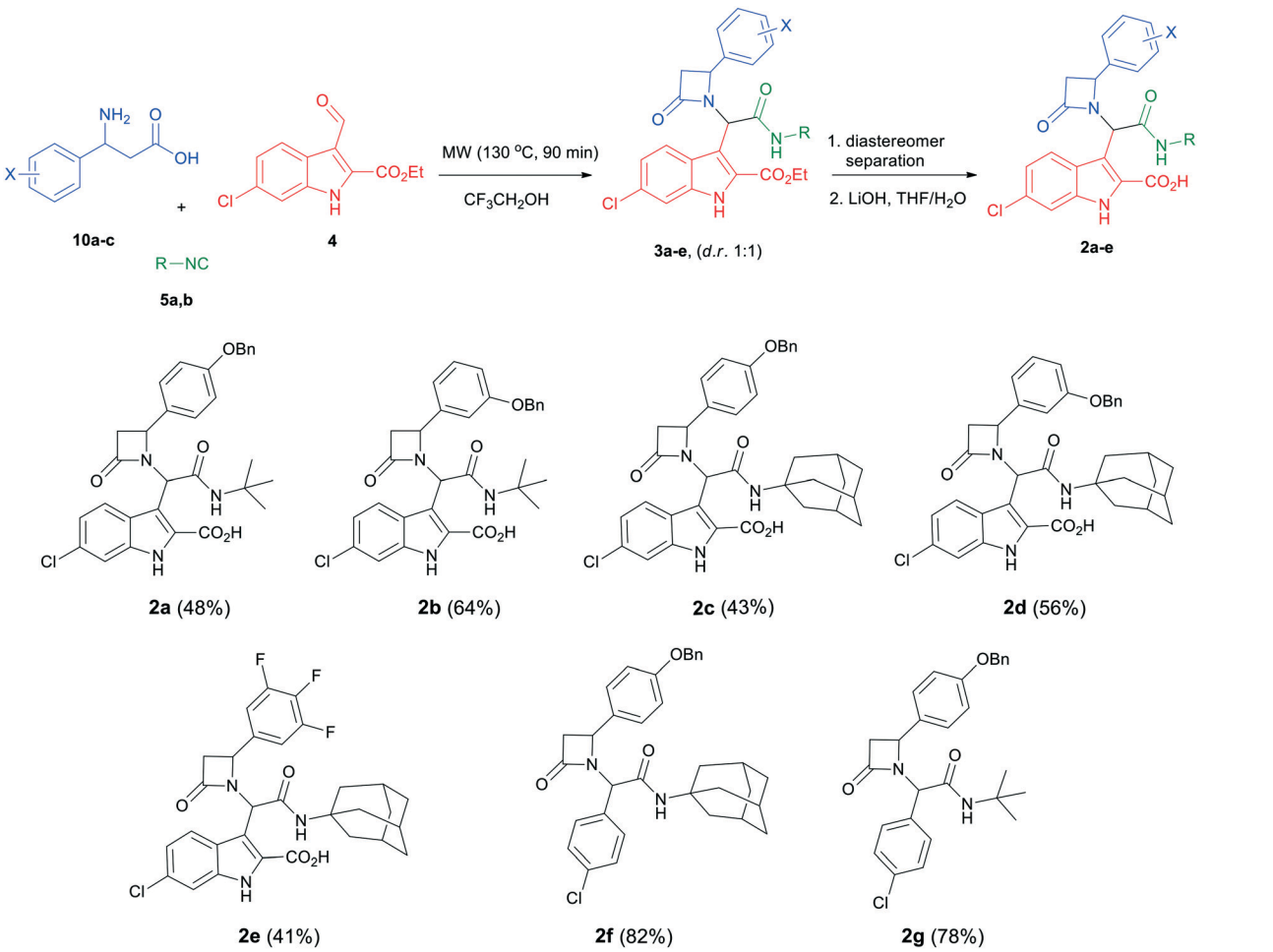

Scheme 3 General reaction scheme and the synthesized library of β-lactams along with the final yields (Ugi-β-lactam and hydrolysis reactions).

in Table 1. To our delight, our designed and synthesized lactams were active against both MDM2 and MDMX, and in some cases, even below 1 μM (entries 3–5). As expected, in most of the cases, one diastereomer showed better affinity than the other one and this was, in all cases, diastereomer B. The configuration of the two different diastereomers could be assigned based on the two protons on the chiral atoms by ^{1}H NMR. Thus, in the case of diastereomer A, the proton on the lactam ring adjacent to nitrogen (H-19) appears at approximately δ 4.40–4.42, compared with diastereomer B in which the H-19 appears higher at δ 4.68–4.83. Moreover, the proton on the chiral carbon adjacent to the amide (H-11) shows resonances at δ 6.20–6.24 and 6.45–6.48 for diastereomers A and B, respectively. *Para*-Substituted phenyl lactams gave slightly better results compared with the *meta*-substituted ones and bulkier isocyanides seem to also contribute to better affinities. Compounds **2c**–**2e** showed similar activity, from which one diastereomer of lactam **2e** demonstrated an affinity of 200 nM. Compounds **2a**, **2c** and **2d** showed notable activity against MDMX as well, an interesting feature that most of the current inhibitors fail to exhibit.[5,26] Compounds **2f** and **2g** with different anchors did not show any activity.

FP-based screening of protein–protein interactions often gives a high fraction of false positives especially with hydrophobic molecules, and therefore it is highly advisable to run a second orthogonal biophysical assay. As a second orthogonal screening system, we performed ^{1}H-^{15}N Heteronuclear Multiple Quantum Correlation (HMQC) NMR experiments.[33,34]

This method is based on the monitoring of chemical shift changes in protein amide backbone resonances upon protein interaction with a small molecule. It allows not only qualitative evaluation of evidence of interaction but also semi-quantitative estimation of the binding affinity. For this NMR experiment, the uniformly ^{15}N-labeled MDM2 was titrated with increasing concentration of the evaluated compound and ^{1}H-^{15}N HMQC spectra were recorded after each new portion of the compound has been added. In the course of the titration, shifts of the cross-peaks assigned to the amino acid

Table 1 Activities of the synthesized library of β-lactam-based inhibitors of p53-MDM2/X interaction

			K_i [μM]			
			MDM2		MDMX	
Entry	Compound	Structure	Diastereomer A	Diastereomer B	Diastereomer A	Diastereomer B
1	**2a**	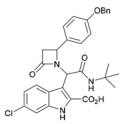	3.2	1.2	12.8	2.1
2	**2b**	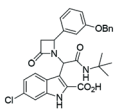	2.1	1.9	2.6	6.7
3	**2c**	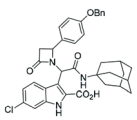	1.9	0.4	4.7	1.4
4	**2d**	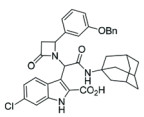	0.9	0.6	2.2	2.6
5	**2e**	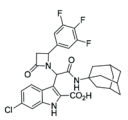	2.0	0.2	—	4.2
6	**2f**	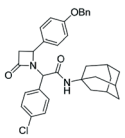	n.a.	n.a.	n.a.	n.a.
7	**2g**	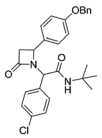	n.a.	n.a.	n.a.	n.a.

n.a. - No activity against MDM2/X protein. K_i values were calculated based on fluorescence polarization binding assay (see the ESI). Diastereomers A and B were defined by ^{1}H NMR. Nutlin-3**a** (positive control for MDM2) K_i = 0.04 μM. Peptide Z (positive control for MDMX) K_i = 0.49 μM.

affected by the binding of the small molecule, *e.g.* Gly58 of MDM2, are observed. Moreover, the strong binding of the compound to the target protein results in NMR signal doubling, indicating K_d values of less than 1 μM (and a slow chemical exchange). Such results were observed in the spectra of ^{15}N-labeled MDM2 titrated with compound **2e** (Fig. 3). In the titration step where the molar ratio of protein : ligand was 5 : 1, the resonance peak doubling was visible (the first signal from the doubled peak remained in the position of the reference peak, while the second – shifted to another position; inset in Fig. 3). This observation is a confirmation of the tight binding of this inhibitor to MDM2 ($K_d < 1$ μM). When the protein : ligand ratio reached 1 : 1, the peak shifted to the position of the second split signal. Assignment of the amide groups of MDM2 was obtained from Stoll *et al.*[35]

Modeling

Despite extensive trials, we were not able to grow crystals of more affine compounds **2c**, **d**, and **e** with MDM2. For that reason, we tried to rationalize the affinity findings using computational modeling using MOLOC[36] and SCORPION.[17] The most active compound of the β-lactam series is **2e** which incorporates a simple trifluoro-substituted benzene moiety. It thus resembles the previously described α-aminoacylamide **11**.[6] Therefore, we used the corresponding cocrystal structure to model **2e** using MOLOC (Fig. 4). To rationalize qualitatively the binding interactions of compounds **2e** and **11** with MDM2, we used the small network analysis software SCORPION (Fig. 4). Compounds **2e** and **11** show very similar interactions with the receptor, including hydrophobic, hydrogen bonding and electrostatic interactions. The bulkier adamantyl residue of **2e** compared to **11** is making more hydrophobic contacts to Met62, Ile61 and Tyr67; for example, **2e** can also make contacts to Val93 whereas **11** is too small to make the corresponding contacts. Notably, the C-3 of the scaffolding β-lactam is also undergoing a short contact to His96. Overall both the binding affinities of **2e** and **11** and the Scorpion scores are very similar.

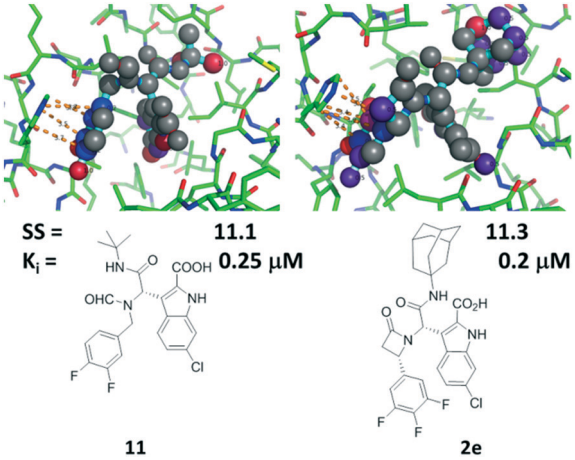

Fig. 4 Comparison of the binding modes of **11** (PDB ID 3TU1) and modeled **2e**. Above: **11** and **2e** in the MDM2 receptor where high scoring atoms are colored red to indicate tight binding. Below: 2D structures of **11** and **2e**, Scorpion scores and binding affinities by FP.

Compounds **2c** and **2d**, with a benzyl elongated ligand moiety, are predicted to bind in a different mode, similar to **1** in our recently described cocrystal structure (Fig. 1A and B).[7] Here again we docked **2c** and **2d** in the crystal structure of **1** and evaluated the ligand receptor complexes using SCORPION (Fig. 5).

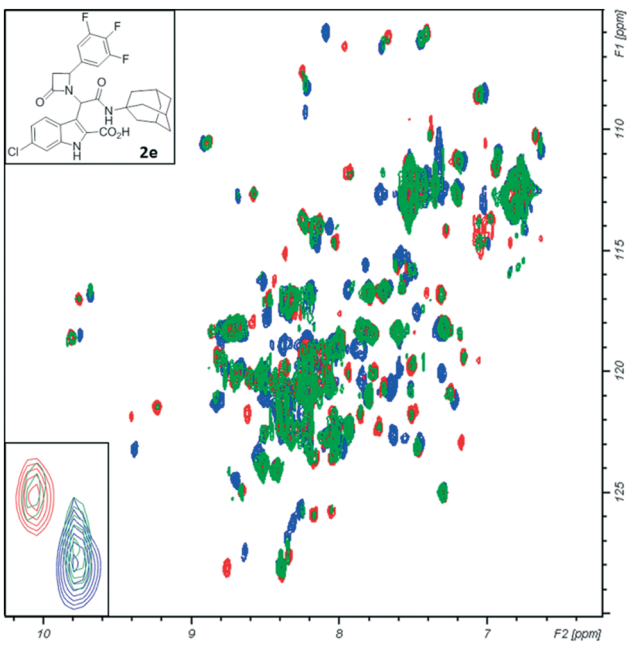

Fig. 3 ^{1}H-^{15}N HMQC titration of MDM2 with **2e**. Blue: reference apo-MDM2 alone; green: the molar ratio of protein/ligand is 5 : 1; red: the molar ratio of protein/ligand is 1 : 1. The enlarged fragment shows resonance peak doubling.

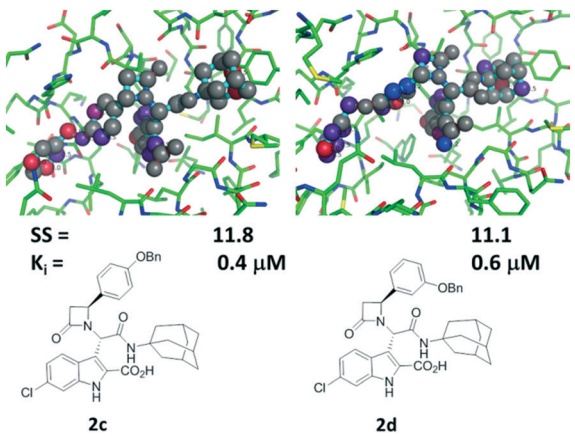

Fig. 5 Comparison of the predicted binding modes of **2c** (PDB ID 3TU1) and **2d** modeled in PDB ID 4MDN. Above: **2c** and **2d** in the MDM2 receptor where high scoring atoms are colored red to indicate tight binding. Below: 2D structures of **2c** and **2d**, Scorpion scores and binding affinities by FP.

The key difference between **2c** and **2d** is their different aromatic substitution patterns, which are *para* and *meta*, respectively. Docking of all four possible stereoisomers make the stereoisomer shown in Fig. 5 most likely, based on predicted interactions using SCORPION analysis. Whereas *meta* substituted **2d** exhibits more hydrophobic contacts in the adamantyl region and also a β-lactam His96 interaction, the interactions in the Leu pocket and the adjacent induced pocket are less compared to **2c**. The bulkier adamantyl moiety has superior contribution to the MDM2 affinity compared to the *tert*-butyl moiety of **1**. However, the adamantyl moiety does not seem to be perfectly shaped complementary to the hydrophobic pocket formed by Val93, Val75, His75, Gln72, Tyr67, Il61 and Met62. Therefore, changing the hydrophobic isocyanide building blocks in this position seems to be an attractive possibility to improve the affinity of similar molecules. The second aromatic group including the two linker atoms of **2c** can make more and stronger hydrophobic contacts in the induced pocket. For example, the two *meta*-C of the second aromatic group exhibit multiple van der Waals interactions with Ile19 and Tyr100. The predicted binding mode is confirmed by the 2D NMR data.

Conclusions

Using our pharmacophore platform ANCHOR.QUERY, we morphed an α-aminoacylamide into a β-lactam scaffold, both of which are potent antagonists of the protein–protein interaction in p53-MDM2. Several predicted compounds were resynthesized using a union of two multicomponent reactions: α-aminoalkylation of the synthesized β-amino acids and Ugi-4CR. Their binding behavior was examined by the use of two orthogonal screening methods, namely, FP and 2D-HSQC. The most potent racemic compound **2e** binds with 200 nM affinity to MDM2. Surprisingly, the compounds show dual action activity against MDM2 and MDMX, with a factor of only 2–4. Overall, this small library of β-lactams gives an initial idea of the activity of this new scaffold and serves as an excellent starting point for further and more extensive SARs. Modeling studies were used to understand the observed SAR. We believe the herein employed process will be useful in scaffold morphing for other PPI targets as well. Studies are ongoing to investigate the MDM2 protein dynamics in the presence of different β-lactams to learn more about the intrinsically disordered MDM2 terminus and what the rules of stabilization are.

Experimental

General procedures, results of fluorescence polarization binding and NMR studies, characterization data, and exemplary copies of NMR spectra are given in the ESI.‡

Acknowledgements

S. Shaabani acknowledges a scholarship from the Ministry of Science, Research and Technology, Tehran, Iran. The work was financially supported by the NIH (2R01GM097082-05) and by the European Union's Horizon 2020 research and innovation programme under MSC ITN "Accelerated Early staGe drug dIScovery" (AEGIS), grant agreement No. 675555.

Notes and references

1 Y. Hu, D. Stumpfe and J. Bajorath, *J. Med. Chem.*, 2017, **60**(4), 1238–1246.
2 G. Schneider, W. Neidhart, T. Giller and G. Schmid, *Angew. Chem., Int. Ed.*, 1999, **38**, 2894–2896.
3 A. Czarna, B. Beck, S. Srivastava, G. M. Popowicz, S. Wolf, Y. Huang, M. Bista, T. A. Holak and A. Dömling, *Angew. Chem., Int. Ed.*, 2010, **49**, 5352–5356.
4 D. Koes, K. Khoury, Y. Huang, W. Wang, M. Bista, G. M. Popowicz, S. Wolf, T. A. Holak, A. Dömling and C. J. Camacho, *PLoS One*, 2012, **7**, e32839.
5 G. M. Popowicz, A. Dömling and T. A. Holak, *Angew. Chem., Int. Ed.*, 2011, **50**, 2680–2688.
6 Y. Huang, S. Wolf, D. Koes, G. M. Popowicz, C. J. Camacho, T. A. Holak and A. Dömling, *ChemMedChem*, 2012, **7**, 49–52.
7 M. Bista, S. Wolf, K. Khoury, K. Kowalska, Y. Huang, E. Wrona, M. Arciniega, G. M. Popowicz, T. A. Holak and A. Dömling, *Structure*, 2013, **21**, 2143–2151.
8 Y. Huang, S. Wolf, B. Beck, L.-M. Köhler, K. Khoury, G. M. Popowicz, S. K. Goda, M. Subklewe, A. Twarda, T. A. Holak and A. Dömling, *ACS Chem. Biol.*, 2014, **9**, 802–811.
9 E. Surmiak, A. Twarda-Clapa, K. M. Zak, B. Musielak, M. D. Tomala, K. Kubica, P. Grudnik, M. Madej, M. Jablonski, J. Potempa, J. Kalinowska-Tluscik, A. Dömling, G. Dubin and T. A. Holak, *ACS Chem. Biol.*, 2016, **11**, 3310–3318.
10 W. Wang, H. Cao, S. Wolf, M. S. Camacho-Horvitz, T. A. Holak and A. Dömling, *Bioorg. Med. Chem.*, 2013, **21**, 3982–3995.
11 A. Dömling, W. Wang and K. Wang, *Chem. Rev.*, 2012, **112**, 3083–3135.
12 A. Dömling, *Chem. Rev.*, 2006, **106**, 17–89.
13 A. Dömling, *Curr. Opin. Chem. Biol.*, 2008, **12**, 281–291.
14 K. Ding, Y. Lu, Z. Nikolovska-Coleska, G. Wang, S. Qiu, S. Shangary, W. Gao, D. Qin, J. Stuckey, K. Krajewski, P. P. Roller and S. Wang, *J. Med. Chem.*, 2006, **49**, 3432–3435.
15 G. W. Bemis and M. A. Murcko, *J. Med. Chem.*, 1996, **39**, 2887–2893.
16 A. Dömling and Y. Huang, *Synthesis*, 2010, 2859–2883.
17 B. Kuhn, J. E. Fuchs, M. Reutlinger, M. Stahl and N. R. Taylor, *J. Chem. Inf. Model.*, 2011, **51**, 3180–3198.
18 I. Ugi and C. Steinbrückner, *Angew. Chem.*, 1960, **72**, 267–268.
19 M. González-López and J. T. Shaw, *Chem. Rev.*, 2009, **109**, 164–189.
20 N. Castagnoli, *J. Org. Chem.*, 1969, **34**, 3187–3189.
21 O. Doebner, *Ber. Dtsch. Chem. Ges.*, 1887, **20**, 277–281.
22 A. M. Van Leusen, J. Wildeman and O. H. Oldenziel, *J. Org. Chem.*, 1977, **42**, 1153–1159.

23 P. Furet, P. Chène, A. De Pover, T. S. Valat, J. H. Lisztwan, J. Kallen and K. Masuya, *Bioorg. Med. Chem. Lett.*, 2012, **22**, 3498–3502.
24 T. Zarganes-Tzitzikas, A. L. Chandgude and A. Dömling, *Chem. Rec.*, 2015, **15**, 981–996.
25 G. Cardillo, L. Gentilucci, A. Tolomelli and C. Tomasini, *J. Org. Chem.*, 1998, **63**, 2351–2353.
26 N. Estrada-Ortiz, C. G. Neochoritis and A. Dömling, *ChemMedChem*, 2016, **11**, 757–772.
27 K. Khoury, G. M. Popowicz, T. A. Holak and A. Dömling, *MedChemComm*, 2011, **2**, 246–260.
28 E. Surmiak, C. G. Neochoritis, B. Musielak, A. Twarda-Clapa, K. Kurpiewska, G. Dubin, C. Camacho, T. A. Holak and A. Dömling, *Eur. J. Med. Chem.*, 2017, **126**, 384–407.
29 C. García-Echeverría, P. Chène, M. J. J. Blommers and P. Furet, *J. Med. Chem.*, 2000, **43**, 3205–3208.
30 M. R. Bauer and F. M. Boeckler, *Structure*, 2013, **21**, 2095–2097.
31 X. Huang, *J. Biomol. Screening*, 2003, **8**, 34–38.
32 A. Czarna, G. M. Popowicz, A. Pecak, S. Wolf, G. Dubin and T. A. Holak, *Cell Cycle*, 2009, **8**, 1176–1184.
33 L. Fielding, *Prog. Nucl. Magn. Reson. Spectrosc.*, 2007, **51**, 219–242.
34 E. Barile and M. Pellecchia, *Chem. Rev.*, 2014, **114**, 4749–4763.
35 R. Stoll, C. Renner, S. Hansen, S. Palme, C. Klein, A. Belling, W. Zeslawski, M. Kamionka, T. Rehm, P. Mühlhahn, R. Schumacher, F. Hesse, B. Kaluza, W. Voelter, R. A. Engh and T. A. Holak, *Biochemistry*, 2001, **40**, 336–344.
36 P. R. Gerber and K. Müller, *J. Comput.-Aided Mol. Des.*, 1995, **9**, 251–268.

